The Moment Equations of Chromatography for Monolithic Stationary Phases

Kanji Miyabe[†] and Georges Guiochon*[,‡]

Faculty of Education, Toyama University, 3190, Gofuku, Toyama 930-8555, Japan, Department of Chemistry, The University of Tennessee, Knoxville, Tennessee 37996-1600, and Division of Chemical and Analytical Sciences, Oak Ridge National Laboratory, Oak Ridge, Tennessee 37831

Received: February 27, 2002; In Final Form: June 13, 2002

The solution in the Laplace domain of the system of equations of the general kinetic model of chromatography provides equations relating the first absolute moment and the second central moment of elution bands to the characteristics of the retention equilibrium and the mass transfer kinetics, respectively. For continuous porous rod (i.e., monolithic) columns, these moment equations have the same form as those for conventional columns packed with spherical particles of a suitable packing material. However, some of the coefficients in the equation of the second central moment are different for conventional and monolithic columns. The results of the calculations made with the moment equations derived here for monolithic columns agree well with some typical characteristics of the experimental behavior observed for monolithic columns, showing the validity of these new moment equations. They should be useful for a detailed analysis of the retention equilibrium and of the mass transfer kinetics in monolithic-type columns. These moment equations are also applicable to the study of the adsorption characteristics of cylindrical adsorbents, such as activated carbon fibers.

Introduction

In the past few years, continuous porous media have become available and proved to be sufficiently reliable, flexible, and affordable systematically to be used as stationary phases to perform chromatographic separations.[1−15] Many recent publications describe high-speed separations carried out with rod-type stationary phases made of monolithic organic polymers[1−8] or inorganic materials.[9−15] These separations can be made with different modes of liquid chromatography (LC), reversed-phase LC (RPLC), ion-exchange LC, and size exclusion LC. The porous structure of the continuous separation medium allows both a low hydraulic resistance of the column to the mobile phase flow and an enhancement of the mass transfer kinetics across the column. Consequently, monolithic HPLC columns exhibit both a high separation efficiency at high flow velocity and a high permeability.

For instance, Nakanishi et al.[16−18] investigated phase separation phenomena taking place during the hydrolysis and gelation of an alkoxysilane solution containing water-soluble polymers, e.g., sodium polystyrene sulfonate and poly(acrylic acid), and made silica gels having micrometer-range interconnected porous morphologies. Minakuchi et al.[9−14] prepared porous silica rods according to this procedure and applied to RPLC the continuous porous media obtained. Rodlike continuous silica materials have a bimodal porous structure. One mode includes micrometer-size pores and macropores between 0.5 and 8 μm, the other mode, meso- and micropores between 2 and 20 nm. The silica skeleton has an average thickness of 0.3 to 5 μm.[9−14] It has been reported that continuous porous silica materials have chromatographic characteristics that are somewhat different from those of the conventional particulate packing materials. Because of their thin skeleton and of the large diameter of the through-macropores, the monolithic columns allow the achievement of high-speed, high-efficiency separations with only a low back pressure. It is expected that the small and thin structure of the silica skeleton will be advantageous for the high-speed separation of macromolecules.[9−14]

The intrinsic characteristics of organic and inorganic monolithic-type columns are different from those of the conventional HPLC columns packed with spherical particles of packing materials. However, it seems that the physicochemical aspects of the retention behavior are not very different for monolithic media and conventional particulate materials. The several advantageous characteristics of monolithic columns originate more from the speed of molecular migration throughout the beds of these continuous porous stationary phases. Fundamental studies on the mass transfer kinetics in monolithic media are necessary for a better understanding of the advantages and limitations of monolithic columns.

The moment analysis of elution peaks based on the general kinetic model is a useful strategy for studying retention equilibria and mass transfer kinetics in chromatographic columns.[19−28] Previously, we studied this kinetics in RPLC and particularly the mechanism of surface diffusion in the intraparticle space under linear isotherm conditions, using the method of moments.[29−36] It is known that the first absolute moment (μ_1) of the elution peak, corresponding to the peak retention, depends only on the adsorption equilibrium constant (K_a).[19−29] On the other hand, the second central moment (μ_2'), corresponding to band broadening, is the sum of contributions due to the different mass transfer processes in the column, i.e., axial dispersion, external mass transfer, intraparticle diffusion, and the actual adsorption/desorption kinetics. So far, however, moment equations for elution peaks have been derived only for chromato-

[†] Faculty of Education.
[‡] Department of Chemistry and Division of Chemical and Analytical Sciences.

10.1021/jp020555b CCC: $22.00
Published on Web 08/06/2002

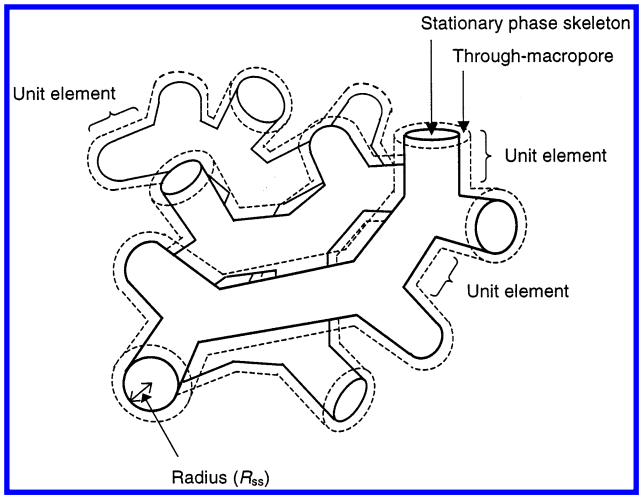

Figure 1. Schematic illustration of the model of the structure of a continuous porous silica rod.

graphic separations using conventional columns, packed with spherical particles of packing materials.[23−28]

The goal of this study is to derive the moment equations for monolithic columns filled with a continuous porous packing material and to calculate some of the chromatographic features of monolithic-type columns using typical values of the parameters included in the new moment equations. The calculated results are compared with those obtained in similar hypothetical calculations made for the conventional particulate columns and with experimental observations previously reported.[2,9−15]

Theory

Fundamental Assumptions Made for the Derivation of the Moment Equations. As shown in scanning electron micrographs available in the literature,[2,9−18] continuous porous media have a complicated structure. Monolithic silica rods have a spongy-like structure with thin silica membranes surrounding large through-macropores. This structure extends across the whole column.[9−18] Because this morphology is very complicated and tortuous, it is difficult clearly to define it. In this study, we assumed as a first approximation that the following hypothetical structure is a proper representation of a porous silica rod for the purpose of modeling mass transfer across it (see Figure 1):

(1) the unit element of the stationary phase skeleton is a porous cylinder containing the mesopores and located in the center of a coaxial, cylindrical through-macropore,

(2) the mobile phase flows through this through-macropore, and

(3) this structure, consisting of a cylindrical skeleton surrounded by a through-macropore, develops in all directions, with anastomosis of the through-macropores. The size of the unit element was estimated from the physical properties of the monolithic column, e.g., the average diameter of the through-macropores and the void fraction of the column.

The system of equations, i.e., the mass balance and the mass transfer kinetic equations in the monolithic column, are based on the following set of assumptions:[23]

(1) The column is radially homogeneous. There is no radial dispersion of the sample.

(2) The mobile phase is incompressible. None of the parameters (e.g., the coefficients of the isotherm, the mobile phase viscosity) is pressure dependent.

(3) The axial dispersion coefficient is constant.

(4) The partial molar volume of the sample components is constant.

(5) The mobile phase is not adsorbed on the stationary phase.

(6) The column is isothermal.

(7) Chromatographic separations are carried out under linear isotherm conditions.

(8) The stationary phase is physicochemically homogeneous. It is located at the center of the through-macropores. As described above, its local shape is assumed to be a cylinder. Note, however, that the cylindrical element of stationary phase should not be considered as straight since the through-macropores are tortuous.

(9) The through-macropores are uniform and have a tortuous cylindrical shape with a constant diameter. The void space surrounding the stationary phase cylinder has the cross-sectional area of the through-macropores.

(10) The mobile phase flow is laminar ($Re \ll 1$, creeping flow, Re = Reynolds number.).

Basic Equations of the General Kinetic Model in Chromatography. The general kinetic model of chromatography includes the mass balance equations of the sample compound in the column and in the stationary phase, and the kinetic equations describing the mass transfer between these three phases,[23,37] i.e., (1) the surface of the stationary phase skeleton, (2) the bulk mobile phase flowing along the through-macropores surrounding the stationary phase, and (3) the mobile phase stagnant inside the mesopores in the stationary phase skeleton. These equations are[23,24,26,27]

$$D_L \frac{\partial^2 C}{\partial z^2} - u\frac{\partial C}{\partial z} - \frac{A_s}{\epsilon} N_0 = \frac{\partial C}{\partial t} \tag{1}$$

$$N_0 = k_f(C - C_{i,R_{ss}}) = D_e\left(\frac{\partial C_i}{\partial r}\right)_{R_{ss}} \tag{2}$$

$$D_e\left(\frac{\partial^2 C_i}{\partial r^2} + \frac{1}{r}\frac{\partial C_i}{\partial r}\right) - N_i = \epsilon_p \frac{\partial C_i}{\partial t} \tag{3}$$

$$N_i = (1 - \epsilon_p)\frac{\partial q}{\partial t} = (1 - \epsilon_p)k_a\left(C_i - \frac{q}{K_a}\right) \tag{4}$$

where C is the concentration of the sample compound in the through-macropore space, z the longitudinal distance along the column, t the time, D_L the axial dispersion coefficient, u the average interstitial velocity of the mobile phase, A_s the ratio of the surface area of the stationary phase skeleton to the column volume, ϵ the column void fraction (external porosity), N_0 the mass flux of the sample compound from the mobile phase to the external surface of the stationary phase skeleton, C_i the concentration of the sample compound within the mesopores inside the stationary phase, R_{ss} the radius of the cylindrical stationary phase skeleton, r the radial distance from the center of the stationary phase cylinder, k_f the external mass transfer coefficient, D_e the diffusion coefficient of the sample compound in the pore space inside the stationary phase skeleton, N_i the mass flux of the sample compound from the stagnant mobile phase in the mesopore space to the surface of the stationary phase, ϵ_p the internal porosity of the stationary phase skeleton, q is the sample concentration adsorbed on the stationary phase, k_a the adsorption rate constant, and K_a the adsorption equilibrium constant.

Solution in the Laplace Domain. The Laplace transform of eqs 1−4 are written as follows:

$$D_L \frac{\partial^2 \bar{C}}{\partial z^2} - u \frac{\partial \bar{C}}{\partial z} - \frac{A_s}{\epsilon} \bar{N}_0 = p\bar{C} \tag{5}$$

$$\bar{N}_0 = k_f(\bar{C} - \bar{C}_{i,R_{ss}}) = D_e\left(\frac{\partial \bar{C}_i}{\partial r}\right)_{R_{ss}} \tag{6}$$

$$D_e\left(\frac{\partial^2 \bar{C}_i}{\partial r^2} + \frac{1}{r}\frac{\partial \bar{C}_i}{\partial r}\right) - \bar{N}_i = \epsilon_p p \bar{C}_i \tag{7}$$

$$\bar{N}_i = (1 - \epsilon_p) p \bar{q} = (1 - \epsilon_p) k_a\left(\bar{C}_i - \frac{\bar{q}}{K_a}\right) \tag{8}$$

where p is the Laplace transform variable and the bar over C, C_i, N_0, N_i, and q denotes the Laplace transforms of C, C_i, N_0, N_i, and q, respectively. The following equation describing the correlation between $\bar{q}$ and $C_{\bar{i}}$ is derived from the last two members of eq 8.

$$\bar{q} = \frac{k_a \bar{C}_i}{p + \frac{k_a}{K_a}} \tag{9}$$

Substitution of eq 9 in eqs 7 and 8 gives the following differential equation for $C_{\bar{i}}$ as a function of r.

$$D_e\left(\frac{\partial^2 \bar{C}_i}{\partial r^2} + \frac{1}{r}\frac{\partial \bar{C}_i}{\partial r}\right) = A(p)\bar{C}_i \tag{10}$$

where

$$A(p) = (1 - \epsilon_p)\frac{p k_a K_a}{p K_a + k_a} + \epsilon_p p \tag{11}$$

A solution for $C_{\bar{i}}$ from eq 10 in terms of $B(z)$ is as follows:

$$\bar{C}_i = B(z) C_1 I_0(r\sqrt{B(p)}) \tag{12}$$

where

$$B(p) = \frac{A(p)}{D_e} \tag{13}$$

$B(z)$ is an arbitrary function of z that will be evaluated later, C_1 is an arbitrary constant, and $I_0(x)$ is the modified Bessel function of zeroth order.

The concentration of the sample compound in the through-macropore space is estimated by substituting eq 12 into the last two members of eq 6.

$$\bar{C} = B(z) C_1 F(p) \tag{14}$$

where

$$E(p) = R_{ss}\sqrt{B(p)} \tag{15}$$

$$F(p) = \frac{E(p)}{B_i} I_1(E(p)) + I_0(E(p)) \tag{16}$$

$$Bi = \frac{k_f R_{ss}}{D_e} \tag{17}$$

and where $I_1(x)$ is the modified Bessel function of the first order. The values of $\bar{C}_i$ and $(\partial \bar{C}_i/\partial r)$ at $r = R_{ss}$ are calculated using eq 12. Substituting these results and $\bar{C}$ from eq 14 into eq 6 gives $\bar{N}_0$ as a function of z.

$$N_0 = D_e B(z) C_1 \sqrt{B(p)} I_1(E(p)) \tag{18}$$

The following equation is derived by substituting eqs 14 and 18 into eq 5.

$$D_L \frac{\partial^2 B(z)}{\partial z^2} - u \frac{\partial B(z)}{\partial z} - G(p) B(z) = 0 \tag{19}$$

where

$$G(p) = p + \frac{A_s k_f}{\epsilon}\left[1 - \frac{I_0(E(p))}{F(p)}\right] \tag{20}$$

The solution of eq 19 gives

$$B(z) = B_0 \exp[-M(p)z] \tag{21}$$

where B_0 is the integration constant and

$$M(p) = \frac{u}{2D_L}\left[\sqrt{1 + \frac{4D_L}{u^2}G(p)} - 1\right] \tag{22}$$

The concentration of the sample compound in the through-macropore space is derived from eqs 14 and 21 as follows:

$$\bar{C} = B_0 \exp[-M(p)z] C_1 F(p) \tag{23}$$

B_0 is determined from the boundary condition at the column inlet ($z = 0$). When a rectangular pulse of time width t is introduced into the column, the boundary condition in the Laplace domain is

$$z = 0; \quad C = \frac{C_0}{p}[1 - \exp(-pT)] \tag{24}$$

where C_0 is the pulse concentration. For an impulse injection, $t \rightarrow 0$ and eq 24 becomes

$$z = 0; \quad \bar{C} = C_0 T \tag{25}$$

Combining eqs 23 and 24 gives the solution of C in the Laplace domain.

$$\bar{C} = \frac{C_0}{p}[1 - \exp(-pT)] \exp[-M(p)z] \tag{26}$$

Moments of the Chromatographic Peaks. From the solution in the Laplace domain, the nth moment of a chromatographic peak is

$$m_n = (-1)^n \lim_{p \rightarrow 0}\left[\frac{d^n}{dp^n}\bar{C}\right] \tag{27}$$

where

$$m_n = \int_0^\infty C t^n dt \tag{28}$$

The nth absolute moment (μ_n) and the central moment (μ_n') are

$$\mu_n = \frac{m_n}{m_0} = \frac{\int_0^\infty Ct^n \, dt}{\int_0^\infty C \, dt} \tag{29}$$

$$\mu_n' = \frac{\int_0^\infty C(t-\mu_1)^n \, dt}{\int_0^\infty C \, dt} = \sum \binom{n}{i} \mu_i (-\mu_1)^{n-i} \tag{30}$$

Zeroth Moment. The zeroth moment (μ_0) as defined in eq 29 is the ratio of the amount of sample compound detected at the exit of the column to that injected. The former is given by eq 27:

$$\mu_0 = \lim_{p\to 0}[\bar{C}] = C_0 T \exp[-M(p)z] \tag{31}$$

The latter is $C_0 t$, as indicated in eq 25. As a consequence, μ_0 is given by

$$\mu_0 = \lim_{p\to 0} \exp[-M(p)z] \tag{32}$$

The value of μ_0 is thus unity because $M(0) = 0$. In usual chromatography, no conversion of the sample compound due to a chemical reaction takes place during the separation.

First Absolute Moment. From eqs 27, 29, and 31,

$$\mu_1 = \frac{m_1}{m_0} = \frac{(-1)\lim_{p\to 0}\left[\frac{d\bar{C}}{dp}\right]}{\lim_{p\to 0}[\bar{C}]} \tag{33}$$

By substituting eq 26 into eq 27,

$$m_1 = C_0 T \left[\lim_{p\to 0}\left[z\frac{dM(p)}{dp} + \frac{T}{2}\right] \exp[-M(p)z]\right] \tag{34}$$

Differentiating the function $M(p)$ with respect to p and taking the limit gives

$$\frac{dM(p)}{dp} = \frac{1}{uN(p)}\left[\frac{dG(p)}{dp}\right] \tag{35}$$

where

$$N(p) = \left[1 + \frac{4D_L}{u^2}G(p)\right]^{1/2} \tag{36}$$

μ_1 is derived as follows from eqs 33−36 along with μ_0 in eq 31.

$$\mu_1 = \left(\frac{z}{u}\right)\lim_{p\to 0}\left[\frac{dG(p)}{dp}\right] + \left(\frac{T}{2}\right) \tag{37}$$

where

$$\lim_{p\to 0}\left[\frac{dG(p)}{dp}\right] = 1 + \frac{A_s R_{ss}}{2\epsilon}[\epsilon_p + (1-\epsilon_p)K_a] \tag{38}$$

Second Central Moment. The second absolute moment (μ_2) is derived similarly, from eqs 27 and 29.

$$\mu_2 = \frac{m_2}{m_0} = \frac{\lim_{p\to 0}\left[\frac{d^2\bar{C}}{dp^2}\right]}{\lim_{p\to 0}[\bar{C}]} \tag{39}$$

By substituting eq 26 into eq 27,

$$m_2 = C_0 T \exp[-M(p)z]\left[\frac{T^2}{3} + Tz\lim_{p\to 0}\left[\frac{dM(p)}{dp}\right] + z^2\left[\lim_{p\to 0}\left[\frac{dM(p)}{dp}\right]\right]^2 - z\lim_{p\to 0}\left[\frac{d^2M(p)}{dp^2}\right]\right] \tag{40}$$

μ_2 is calculated from eqs 31, 39, and 40.

$$\mu_2 = \frac{T^2}{3} + TZ\lim_{p\to 0}\left[\frac{dM(p)}{dp}\right] + z^2\left[\lim_{p\to 0}\left[\frac{dM(p)}{dp}\right]\right]^2 - z\lim_{p\to 0}\left[\frac{d^2M(p)}{dp^2}\right] \tag{41}$$

According to its definition (eq 30), the second central moment (μ_2') is derived from eqs 41 and 37.

$$\mu_2' = \mu_2 - {\mu_1}^2 = \frac{T^2}{12} - z\lim_{p\to 0}\left[\frac{d^2M(p)}{dp^2}\right] \tag{42}$$

Similar to eq 35, differentiating $[dM(p)/dp]$ with respect to p and taking the limit gives

$$\frac{d^2M(p)}{dp^2} = -\frac{2D_L}{u^3[N(p)]^3}\left[\frac{dG(p)}{dp}\right]^2 + \frac{1}{uN(p)}\frac{d^2G(p)}{dp^2} \tag{43}$$

μ_2' is derived from eqs 42 and 43.

$$\mu_2' = \left(\frac{z}{u}\right)\left[\left(\frac{2D_L}{u^2}\right)\frac{\left[\lim_{p\to 0}\left[\frac{dG(p)}{dp}\right]\right]^2}{[\lim_{p\to 0}[N(p)]]^3} - \frac{\lim_{p\to 0}\left[\frac{d^2G(p)}{dp^2}\right]}{\lim_{p\to 0}[N(p)]} + \frac{T^2}{12}\right] \tag{44}$$

where

$$\lim_{p\to 0}\left[\frac{d^2G(p)}{dp^2}\right] = \frac{A_s R_{ss}}{\epsilon}\left[(1-\epsilon p)\frac{{K_a}^2}{k_a} + \left(\frac{R_{ss}}{2k_f} + \frac{{R_{ss}}^2}{8D_e}\right)[\epsilon_p + (1-\epsilon_p)K_a]^2\right] \tag{45}$$

Moment Equations. In summary, the zeroth moment, the first absolute moment, and the second central moment are represented as follows:

$$\mu_0 = 1 \tag{46}$$

$$\frac{\mu_1 - \frac{T}{2}}{\frac{z}{u}} = \left[1 + \frac{1-\epsilon}{\epsilon}[\epsilon_p + (1-\epsilon_p)K_a]\right] \tag{47}$$

$$\frac{\mu_2' - \frac{T^2}{12}}{\frac{z}{u}} = \frac{2D}{u^2}\left[1 + \frac{1-\epsilon}{\epsilon}[\epsilon_p + (1-\epsilon_p)K_a]\right]^2 + \frac{2(1-\epsilon)}{\epsilon}\left[(1-\epsilon_p)\frac{{K_a}^2}{k_a} + \left(\frac{R_{ss}}{2k_f} + \frac{{R_{ss}}^2}{8D_e}\right)[\epsilon_p + (1-\epsilon_p)K_a]^2\right] \tag{48}$$

where $A_s R_{ss} = 2(1-\epsilon)$. These equations demonstrate how several fundamental parameters contribute together to influence the shape of the elution peak profiles under linear isotherm

conditions. The peak position depends on only one equilibrium parameter, K_a (eq 47). On the other hand, the peak broadening is related to K_a and to the four kinetic parameters, D_L, k_a, k_f, and D_e. Equation 48 suggests that these parameters can be derived from experimental results by analyzing the profiles of peaks recorded under different conditions, particularly with different interstitial velocity of the mobile phase (u) and different radius of the cylindrical element of the stationary phase skeleton (R_{ss}).

The formulation of eq 47 is the same as that of the conventional first moment equation derived for chromatographic columns packed with spherical particles of packing material. By contrast, eq 48 is slightly different from the conventional moment equation for μ_2'.[23−29]

$$\frac{\mu_2' - \frac{T^2}{12}}{\frac{z}{u}} = \frac{2D_L}{u^2}\left[1 + \frac{1-\epsilon}{\epsilon}[\epsilon_p + (1-\epsilon_p)K_a]\right]^2 + \frac{2(1-\epsilon)}{\epsilon}\left[(1-\epsilon_p)\frac{K_a^2}{k_a} + \left(\frac{R_p}{3k_f} + \frac{R_p^2}{15D_e}\right)[\epsilon_p + (1-\epsilon_p)K_a]^2\right] \quad (49)$$

where R_p is the radius of the stationary phase particles. One parameter relating to the size of the stationary phase (R_{ss}) and the two coefficients for k_f and D_e in eq 48 are different from those in eq 49. Equations 48 and 49 are derived with different assumptions concerning the structure of the continuous porous packing materials, that is

(1) Equation 48 assumes a unit structure consisting of a cylinder of porous stationary phase located at the center of a through-macropore space.

(2) Equation 49 assumes a unit structure consisting of spherical particles of packing material surrounded by a thin flow of mobile phase.

In both cases, the structure develops homogeneously in all various directions and there is anastomosis of the different channels of the mobile phase. As described earlier, our preliminary model of rod columns is essentially based on the known microstructure of the continuous porous silica monoliths. However, eqs 47 and 48 would also be effective for other monolithic-type columns when the approximate model assumed here describes well the structural characteristics of other continuous porous separation media. This model and its moment equations should be applicable to kinetic studies of the transfer phenomena in cylindrical adsorption media, such as activated carbon fibers or other fiber adsorbents which are used in gas−solid and liquid−solid adsorption and in solid-phase extraction.

Calculation

The characteristics of the chromatographic behavior of a hypothetical monolithic column were calculated by substituting appropriate representative or typical numerical values for the parameters in the moment equations, eqs 47 and 48. The results of these calculations were compared with those obtained for a hypothetical conventional column packed with spherical particles and with experimental data reported in previous papers.[2,9−18]

Table 1 shows some physicochemical properties of the two hypothetical columns. In this first study, the following two types of columns were considered, a monolithic column packed with a continuous porous silica rod and a conventional column packed with spherical silica gel particles. The values of the parameters in Table 1 are typical for silica monolithic columns and for conventional particulate silica gel columns used for RPLC. The values were used in the hypothetical calculations without specific annotation. It was assumed that the average radius of the through-macropores in the continuous porous silica rod was 1.0 μm and that of the diameter of spherical silica gel particles was 2.5 μm.

TABLE 1: Physicochemical Properties of the Hypothetical Monolithic Column and the Conventional Particulate Column and Imaginary Experimental Conditions[a]

	monolithic column	particulate column
average radius of through-macropores (μm)	1.0	
average radius of spherical particles (μm)		2.5
external porosity, ϵ	0.75	0.40
internal porosity, ϵ_p	0.40	0.40
total porosity	0.85	0.64
superficial velocity, u_0 (cm s^{-1})	1.0	1.0
adsorption equilibrium constant, K_a	10	10
molecular diffusivity, D_m (cm^2 s^{-1})	1×10^{-5}	1×10^{-5}
pore diffusivity, D_p (cm^2 s^{-1})	1×10^{-6}	1×10^{-6}
Surface diffusion coefficient, D_s (cm^2 s^{-1})	1×10^{-6}	1×10^{-6}

[a] The values listed in this table were used in the hypothetical calculations as typical values without specific annotation.

Structure of the Continuous Porous Silica Rod. The silica monolithic stationary phase has a spongelike bimodal pore structure consisting of through-macropores with a diameter of the order of 1 μm wrapped in a silica skeleton having geometrical dimensions of the same order of magnitude and containing mesopores with diameters of the order of 10 nm inside the silica skeleton.[9−18] Because of the extremely complicated morphology of the continuous porous silica rods, it is difficult clearly to define the microstructure of the monolithic stationary phase. As described earlier (Figure 1), we assumed a simple model of the structure of the rod consisting in a bundle of approximately parallel, slightly twisted cylinders of porous silica containing the mesopores and surrounded by a coaxial, cylindrical through-macropore. These macropores are anastomosed and this permit the flow of the mobile phase and radial mass transfer. The radius of the cylindrical silica skeletons (R_{ss}) and that of the coaxial through-macropores surrounding the silica skeleton were estimated as 0.58 and 1.2 μm, respectively, from the hypothetical parameters listed in Table 1. Under these conditions, the effective cross-sectional area of the macropore space is almost equal to that of the through-macropores with an average diameter of approximately 2.0 μm, in agreement with the value which is experimentally estimated from the scanning electron micrographs.

Kinetic Parameters. The kinetic parameters involved in eqs 48 and 49 were estimated using some common literature correlations.

Axial Dispersion. The axial dispersion coefficient (D_L) was derived assuming that axial dispersion consists of molecular diffusion and eddy diffusion,[23] through the equation

$$D_L = y_1 D_m + y_2 d_p u \quad (50)$$

where D_m is the molecular diffusivity, d_p the particle diameter, u the interstitial velocity of the mobile phase, and γ_1 and γ_2 are geometrical constants whose values were taken as 0.7 and 0.5, respectively.[23] As listed in Table 1, a diameter of 2.0 μm was assumed for the through-macropores, a size which is similar to that of the interstitial voids in conventional columns packed with 5.0 μm spherical particles.[38,39] (although, because the constriction of the channels is much smaller in a rod than in a packed column, the permeability of the former is higher) In

this study, D_L for the hypothetical monolithic column was estimated by assuming a value of $d_p^* = 5.0$ μm in eq 50, a value corresponding to the hypothetical diameter of the through-macropores, i.e., 2.0 μm, in the continuous porous silica rod. For example, the value of D_L given by eq 50 is 4.6×10^{-5} cm^2 s^{-1} for $D_m = 1 \times 10^{-5}$ cm^2 s^{-1} and $u = 0.16$ cm s^{-1}. The value of D_L depends significantly on the column conditions, e.g., on the packing structure of the stationary phase and the fluid flow dispersion of the mobile phase. More accurate information on axial dispersion and the value of D_L could be derived from experimental data by taking advantage of the difference in the flow rate dependence of each contribution to the mass transfer process in monolithic columns. Equations 47 and 48 are useful for this purpose.

External Mass Transfer. The external mass transfer coefficient (k_f) was estimated on the basis of the penetration theory.[40]

$$k_f = \sqrt{\frac{4D_m u}{2\pi R_{ss}}} \tag{51}$$

The value of k_f is calculated as 0.13 cm s^{-1} for $D_m = 1 \times 10^{-5}$ cm^2 s^{-1}, $u = 0.16$ cm s^{-1}, and $R_{ss} = 0.58$ μm. A similar value of k_f (0.12 cm s^{-1}) was derived from the equation proposed by Kataoka et al.[41] under the same conditions.

$$Sh = \frac{k_f(2R_{ss})}{D_m} = 1.85\left(\frac{1-\epsilon}{\epsilon}\right)^{1/3} Re^{1/3} Sc^{1/3} \tag{52}$$

where Sh is the Sherwood number, Re is the Reynolds number ($=2R_{ss}\epsilon u\rho/\eta$), and Sc is the Schmidt number ($=\eta/(\rho D_m)$). On the other hand, k_f is calculated as 0.28 cm s^{-1} under the same conditions when using the Wilson−Geankoplis equation.[42]

$$Sh = \frac{1.09}{\epsilon} Re^{1/3} Sc^{1/3} \tag{53}$$

The external mass transfer should be investigated in more detail because there have been few fundamental studies in chromatography on the external mass transfer process and none yet for monolithic columns.

Mass Transfer inside the Stationary Phase Porous Skeleton. The effective diffusivity in the pores located inside the stationary phase skeleton (D_e) was calculated using the following equation that assumes parallel contributions of pore diffusion and surface diffusion.[24,25]

$$D_e = D_p + (1-\epsilon_p)K_a D_s \tag{54}$$

According to results obtained in previous studies,[29−32] the value of D_p and D_s was assumed to be 1×10^{-6} cm^2 s^{-1}, which is 1 order of magnitude smaller than D_m.

Results and Discussion

Chromatographic separations depend on various factors. For instance, the nature and the concentration of the organic modifier that is used to prepare the mobile phase significantly influence both the retention and the band broadening in RPLC. Their influence on the separation is therefore rather complex. It is difficult to evaluate the influence of only one parameter at a time on the separation behavior by experimental approaches. This is easier by calculations. We attempted to simulate the chromatographic behavior by using the moment equations derived here and to obtain new information on the separation characteristics of monolithic-type columns. The calculation results for the hypothetical monolithic and packed columns were compared together and with data resulting from experimental observations reported in previous papers.[2,9−18]

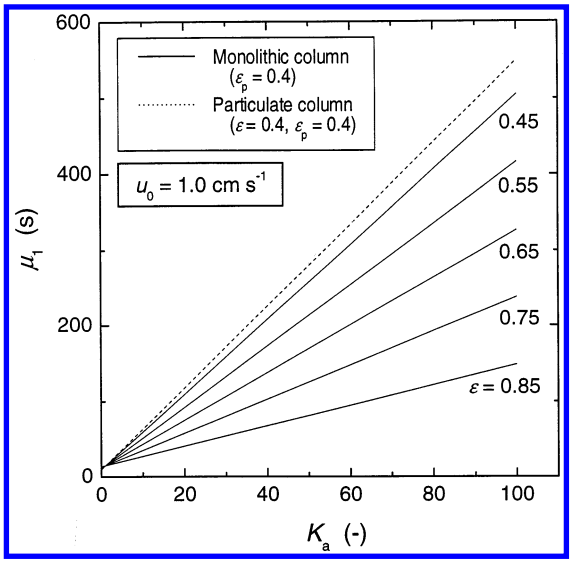

Figure 2. Linear correlation of the first absolute moment with the adsorption equilibrium constant.

Comparison of Retention Strength. Figure 2 shows the calculated correlations of μ_1 with K_a at $u_0 = 1.0$ cm s^{-1}. The value of μ_1 increases linearly with increasing K_a for both types of columns. However, the slope of the straight line obtained for the monolithic column ($\epsilon = 0.75$) is smaller than that for the conventional packed column ($\epsilon = 0.40$) by a factor of about 2.3 under the conditions listed in Table 1. The difference in the slopes of these two straight lines arises from the difference in the volumes of stationary phase contained in the two columns. According to the values of their total porosities (Table 1), the volumetric fractions occupied by the stationary phase are 0.15 and 0.36 for the monolithic and the packed column, respectively. In conclusion, the retention observed on monolithic columns is usually small compared with that on conventional packed columns. This is in agreement with the experimental observations.[9,10,13]

Comparison of the Column Efficiencies. The following plate height equation for monolithic columns is derived from eqs 47, 48, 50, and 51 in the assumption that the contribution of the actual adsorption/desorption kinetics to μ_2' was negligibly small.[43]

$$H = \frac{2y_1 D_m}{u} + 2y_2 d_p^* + \frac{\epsilon R_{ss}^{3/2}}{(1-\epsilon)(1+\delta_0)^2}\left(\frac{\pi}{2D_m}\right)^{1/2} u^{1/2} + \frac{\epsilon R_{ss}^2}{4(1-\epsilon)D_e(1+\delta_0)^2}\frac{\delta_0^2}{u} = H_{ax}^* + H_f^* + H_d^* \tag{55}$$

where

$$\delta_0 = \frac{1-\epsilon}{\epsilon}[\epsilon_p + (1-\epsilon_p)K_a] \tag{56}$$

$$H_{ax}^* = \frac{2y_1 D_m}{u} + 2y_2 d_p^* \tag{57}$$

$$H_f^* = \frac{\epsilon R_{ss}^{3/2}}{(1-\epsilon)}\frac{\delta_0^2}{(1+\delta_0)^2}\left(\frac{\pi}{2D_m}\right)^{1/2} u^{1/2} \tag{58}$$

$$H_d^* = \frac{\epsilon R_{ss}^2}{4(1-\epsilon)D_e(1+\delta_0)^2}\frac{\delta_0^2}{u} \tag{59}$$

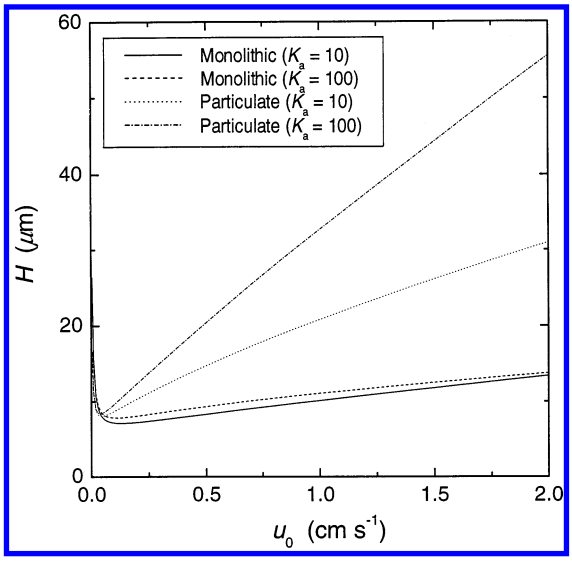

Figure 3. Height equivalent to a theoretical plate as a function of the superficial velocity of the mobile phase.

Equation 55 accounts for the dependence of the height equivalent to a theoretical plate (H) on the mobile phase velocity, u, and is similar to the classical kinetic equations of chromatography such as the van Deemter equation[23,37,44]

$$H = A' + \frac{B'}{u} + C'u \tag{60}$$

Equation 55 is useful to the study of the physicochemical meaning of the coefficients A', B', and C' which are included in kinetic equations such as eq 60.

Figure 3 shows the correlations between H and the superficial velocity of the mobile phase (u_0). Equation 55 was used in the calculations made for the monolithic silica column. Similar calculations were made using another kinetic equation that correlates H and u_0, and which was derived for conventional columns packed with spherical particles of packing materials.

$$H = \frac{2y_1D_m}{u} + 2y_2d_p + \frac{\epsilon^2 d_p}{3.27(1-\epsilon)}\frac{\delta_0^2}{(1+\delta_0)^2}\left(\frac{\epsilon d_p}{D_m}\right)^{2/3} u^{2/3} + \frac{\epsilon^2 d_p^2}{30(1-\epsilon)D_e}\frac{\delta_0^2}{(1+\delta_0)^2} u \tag{61}$$

where

$$H_{ax} = \frac{2y_1D_m}{u} + 2y_2d_p \tag{62}$$

$$H_f = \frac{\epsilon^2 d_p}{3.27(1-\epsilon)}\frac{\delta_0^2}{(1+\delta_0)^2}\left(\frac{\epsilon d_p}{D_m}\right)^{2/3} u^{2/3} \tag{63}$$

$$H_d = \frac{\epsilon^2 d_p^2}{30(1-\epsilon)D_e}\frac{\delta_0^2}{(1+\delta_0)^2} u \tag{64}$$

In Figure 3, the superficial velocity, u_0, is used in the horizontal axis instead of the interstitial velocity, u, because ϵ is markedly different for the two types of columns. The profiles of the curves for the monolithic and the conventional packed columns are almost identical in the low flow velocity range. At high flow velocity, however, a different trend is observed for the two columns in the correlation of H and u_0. As reported previously,[9−13] the increase of H with increasing u_0 is only quite moderate for the monolithic column. By contrast, there is a pronounced increase of H with increasing u_0 for the packed column. The smaller the value of K_a, the stronger the increase of H with increasing u_0. On the other hand, almost identical HETP-curve profiles are calculated for the monolithic column, irrespective of the value of K_a. Ultimately, the optimum flow velocity is slightly larger for the monolithic than for the packed column and the minimum value of H slightly smaller for the monolithic than for the packed column. These results based on our calculations are in excellent agreement with experimental results.[9−13] As shown in Figures 2 and 3, the hypothetical calculations based on eqs 47 and 48 account properly for the separation characteristics of monolithic columns, proving the validity of the new moment equations.

Contribution of Each Mass Transfer Process to Column Efficiency. Figure 3 shows the overall column efficiency as a function of the mobile phase flow velocity. As indicated in eqs 55 and 61, H is the sum of the contributions of the three mass transfer processes in the columns. Usually, the overall column efficiency is the only parameter that can be measured experimentally, the value of each contribution is not directly accessible. Figure 4a,b shows the flow rate dependence of each of the three contributions. As shown in Figure 4a, the curves giving H for the monolithic column are the same at $K_a = 10$ and $K_a = 100$. However, the calculations show also (see Figure 4a) that the relative importance of each contribution is different at $K_a = 10$ and 100.

At $K_a = 10$ and $u_0 < 2.0$ cm s^{-1}, the contribution of axial dispersion (H_{ax}^*) to H is always larger than those of the external mass transfer (H_f^*) and the diffusive mass transfer inside the stationary phase skeleton (H_d^*). Both contributions, H_f* and H_d*, increase similarly with increasing flow rate. They are of the same order of magnitude. On the other hand, at $K_a = 100$, the curves for H_f^* and H_d^* are quite different, the former being much larger than the latter. The contribution of H_f^* is larger at $K_a = 100$ than at $K_a = 10$. By contrast, the contribution of H_d^* decreases with increasing K_a from 10 to 100. No change is predicted for the contribution of H_{ax}^* because the first and second terms in the right-hand side of eq 55 are independent of K_a.

Figure 4b shows the corresponding results, also at $K_a = 10$ and 100, for the hypothetical column packed with spherical particles. The difference between the curves giving H at $K_a = 10$ and 100 arises primarily from the dependence of the contribution of intraparticle diffusion (H_d) to H because the contribution of the external mass transfer (H_f) is almost the same at $K_a = 10$ and 100. The contribution of axial dispersion (H_{ax}) is small compared to those of H_d and H_f. The comparison of the calculation results in Figure 4a,b suggests that the high efficiency of monolithic columns results mainly from the small thickness of the silica skeleton because the contributions of H_f^* and H_d^* to H are smaller for the monolithic than those for the packed column.

According to eq 60, a similar information may be derived by analyzing the flow rate dependence of H. The coefficients A', B', and C' in eq 60 could be calculated by fitting the experimental data H, u_0 to this equation. However, the data analysis based on eq 60 provides only overall values of the three coefficients while these coefficients involve the effects of several parameters, as indicated in eqs 57−59 and 62−64. The individual influence of each these parameters on H cannot be evaluated from the mere analysis of the profile of a single HETP curve. The correlation between H and u_0 must be measured

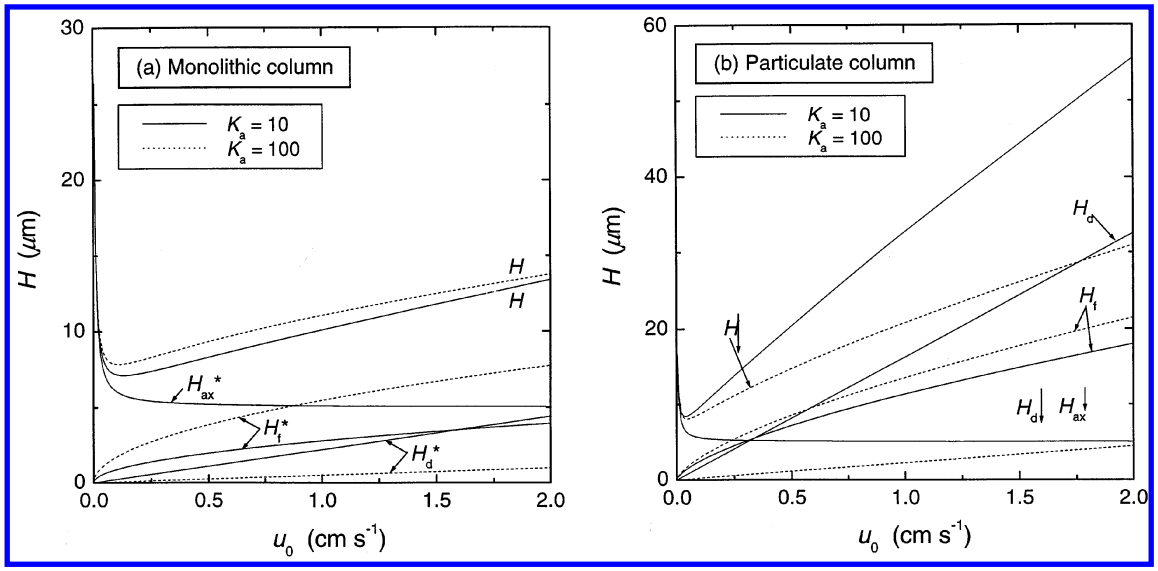

Figure 4. Flow rate dependence of the height equivalent to a theoretical plate (H) and the contributions to H of the axial dispersion (H^*_{ax}, H_{ax}), the external mass transfer (H^*_f, H_f), and the diffusive mass transfer inside the stationary phase (H^*_d, H_d) in (a) the hypothetical monolithic column and (b) the hypothetical conventional particulate column packed with spherical particles.

under different conditions. Iterative measurements of the experimental data have to be tediously repeated while changing the chromatographic conditions. However, except for the flow velocity, it is difficult to change only one experimental parameter at a time, due to the complex interactions between these parameters. Equations 55 and 61 are more useful than eq 60 for analyzing the individual effect of each parameter and for a better understanding of the characteristics of the separation process from a kinetic point of view.

Knox discussed band dispersion in chromatography on the basis of a conventional HETP equation (eq 60) and claimed that the most important contribution to band broadening in HPLC arose in the actual stream of mobile phase.[44] As shown in eq 50, the axial dispersion coefficient (D_L) in eq 48 accounts for the influence on band broadening of both axial molecular diffusion and eddy diffusion. Attempts at relating the values of the coefficients γ_1 and γ_2 to geometrical characteristics of the networks of mesopores (internal porosity) and through- or macropores (external porosity) were made by Giddings,[37] but no convincing result were obtained for the lack of good pore descriptors.[44] If we had enough information on the flow structure in monolithic columns (i.e., on the distribution of the streamlines), we could modify and improve eq 50, hence eq 48, to better account for band broadening phenomena.

The flow profile in monolithic columns is determined by the distribution of the diameters of the through-macropores and of the stationary phase skeleton. No experimental data are available concerning these size distributions. The influence of these distributions on the extent of eddy diffusion is unclear. On the other hand, information is available on the radial distributions of the fluid flow velocity and of the local efficiency for conventional columns.[45−61] Axial and transverse dispersion were also studied in conventional packed columns.[55−58] It has been shown[45] that the persuasive arguments made by Knox[44,46,47] regarding the importance of the contribution to band dispersion that arises in the mobile phase stream was explained by the radial heterogeneity of the column bed due to the friction between this bed and the column tube, during the packing process. There is no similar information nor even any reliable experimental data on the characteristics of mass transfer in monolithic columns, e.g., on the radial distribution of the mobile phase velocity, on transverse dispersion, or on correlations between flow profiles in the continuous porous media and the efficiency of the monolithic columns. The moment equations presented here assume the column to be radially homogeneous. They are but a first step that should be completed later by investigations of the radial heterogeneity of monolithic columns.

Contribution of Each Mass Transfer Process to Band Broadening. It is well-known that H is correlated with μ_1 and μ_2'. The dependence of the HETP curve on u_0 results mostly from the flow rate dependence of μ_2' because μ_1 is merely inversely proportional to u_0. To explain the difference in the profiles of the plots of H, H^*_f, H_f, H^*_d, and H_d in Figure 4a,b, the contributions to μ_2' of the three mass transfer processes in the columns were evaluated and are shown in Figure 5a,b. Figure 5a indicates that, for the monolithic column, the contributions to μ_2' of the external mass transfer (δ^*_f) and of the diffusive mass transfer inside the stationary phase skeleton (δ^*_d) are negligibly small in the low flow velocity range and that, in this range, μ_2' is almost equal to the contribution of axial dispersion (δ^*_{ax}).

$$\delta^*_{ax} = \frac{2zD^*_L}{u^3}(1+\delta_0)^2 \tag{65}$$

$$\delta^*_f = \frac{z\epsilon R_{ss}}{u(1-\epsilon)k_f}\delta_0^2 \tag{66}$$

$$\delta^*_d = \frac{z\epsilon R^2_{ss}}{4u(1-\epsilon)D_e}\delta_0^2 \tag{67}$$

The values of δ^*_{ax}, δ^*_f, and δ^*_d decrease almost linearly with increasing flow velocity. δ^*_{ax} is more sensitive to changes in u_0 than δ^*_f and δ^*_d. The contributions of δ^*_{ax}, δ^*_f, and δ^*_d to μ_2' are almost the same at $u_0 \approx 2.0$ cm s^{-1}. When u_0 is larger than about 2.0 cm s^{-1}, δ^*_d has a predominant contribution to μ_2'. On the other hand, the contribution of δ^*_f to μ_2' is always smaller than that of δ^*_{ax} or δ^*_d. In this study, the external mass transfer coefficient k_f was estimated on the basis of the penetration theory because no correlation has been proposed yet for estimating k_f in a continuous porous packing material.[40] As described earlier, k_f is calculated from eq 51 as equal to 0.13 cm s^{-1} for $D_m = 1$

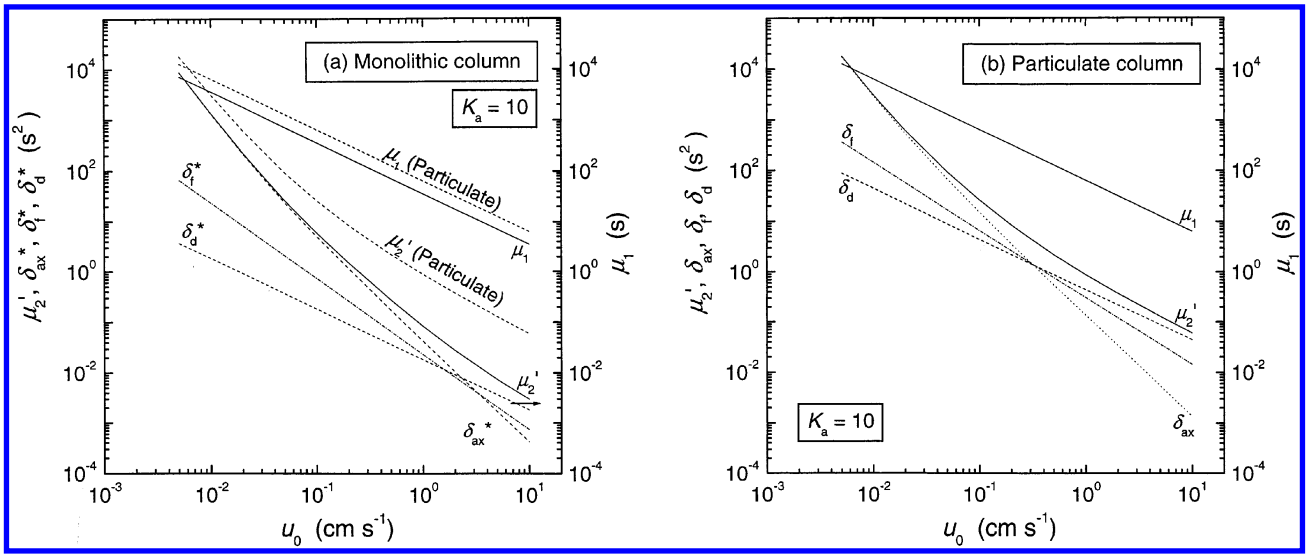

Figure 5. Flow rate dependence of the first absolute moment (μ_1), the second central moment (μ_2'), and the contributions to μ_2' of the axial dispersion (δ_{ax}^*, δ_{ax}), the external mass transfer (δ_f^*, δ_f), and the diffusive mass transfer inside the stationary phase (δ_d^*, δ_d) in (a) the hypothetical monolithic column and (b) the hypothetical conventional particulate column.

$\times 10^{-5}$ cm^2 s^{-1}, $u = 0.16$ cm s^{-1}, and $R_{ss} = 0.58$ μm. Equation 52, proposed by Kataoka et al.,[41] also provides a similar value of k_f (= 0.12 cm s^{-1}) under the same conditions. On the other hand, the corresponding value of k_f calculated from eq 53 (the Wilson-Geankoplis equation[42]) is 0.28 cm s^{-1}, which is different from the values calculated by eqs 51 and 52. However, this difference is small enough and this error does not significantly influence the calculation results in Figure 5a. Figure 5a indicates that the contribution of δ_f^* to μ_2' is several times to almost 1 order of magnitude smaller than that of δ_{ax}^* or δ_d^* in most of the range of u_0 and is about 20−30% at its maximum, for $u_0 \approx 2.0$ cm s^{-1}.

Similarly, Figure 5b shows the results of the calculation of the contribution of the axial dispersion (δ_{ax}), the external mass transfer (δ_f), and the intraparticle diffusion (δ_d) to μ_2' for the conventional column packed with spherical particles. These contributions are

$$\delta_{ax} = \frac{2zD_L}{u^3}(1 + \delta_0)^2 \tag{68}$$

$$\delta_f = \frac{2z\epsilon R_p}{3u(1-\epsilon)k_f}\delta_0^2 \tag{69}$$

$$\delta_d = \frac{2z\epsilon R_p^2}{15u(1-\epsilon)D_e}{\delta_0}^2 \tag{70}$$

Almost the same conclusion would be derived from Figure 5a,b. Two curves illustrating the flow rate dependence of μ_1 and μ_2' for the particulate column are also shown as dotted lines in Figure 5a. The two straight lines for μ_1 are parallel. The difference between the curves giving μ_2' for the two columns increases with increasing u_0. Comparing the calculation results in Figure 5,b shows that the steeper decrease in μ_2' for the monolithic column is mainly due to the lower contributions of δ_d^* and δ_f^* in the high flow velocity range. This result is obviously consistent with the one in Figure 4a,b.

Effect of the Retention Factor on the Column Efficiency. The experimental conditions of chromatographic separations can be optimized by adjusting various parameters. Changing the mobile phase composition is an effective strategy in many cases. It modifies the retention and, as illustrated in Figures 3 and 4b, the efficiency of packed columns increases with increasing K_a. The monolithic and the packed columns exhibit different dependencies of their plate height on the retention factor, H being almost independent of K_a for the monolithic column (Figure 3). However, it is difficult to elucidate the influence of the retention factor on H through experimental measurements because it is not possible to change only K_a while all the other parameters remain constant. The interactions between the different parameters controlling the chromatographic behavior are complex. A theoretical approach is more effective to calculate and predict the behavior of chromatographic processes under changing conditions than an experimental one.

Figure 6a,b shows the correlations between H and K_a calculated for the monolithic and the packed columns, respectively. One of the characteristics of monolithic columns is that H is depends but weakly on either the mobile phase flow velocity (u_0) or the retention (K_a). The results in Figure 6a provide an explanation for these phenomena. The variations with K_a of the contributions H_f^* and H_d^* cancel each other at $K_a >$ 10. In addition, the contribution of H_{ax}^* is independent of K_a and is relatively large compared with the small contributions H_f^* and H_d^*. This suggests that the axial and/or the radial dispersion should be studied in more detail and that their contribution may limit the ultimate efficiency of monolithic columns.

The calculation results in Figure 6b contrast with those in Figure 6a. The efficiency of the packed column increases with increasing retention, irrespective of the flow velocity. As shown in Figure 3, the flow rate dependence of H is larger for the packed column than for the monolithic one. Furthermore, the HETP of the packed column is larger than that of the monolithic column. The HETP curve results from the combination of the small contribution H_{ax} and from the remarkable variations of the two contributions H_d and H_f.

Effect of Diffusivity on Column Efficiency. As described earlier, it is expected that monolithic columns, the bed of which is made of a continuous porous separation medium consisting of a thin stationary phase skeleton, is particularly suitable for the high-speed separation of large molecules.[9−13] Figure 7a,b shows the influence of the diffusivity of the sample compound

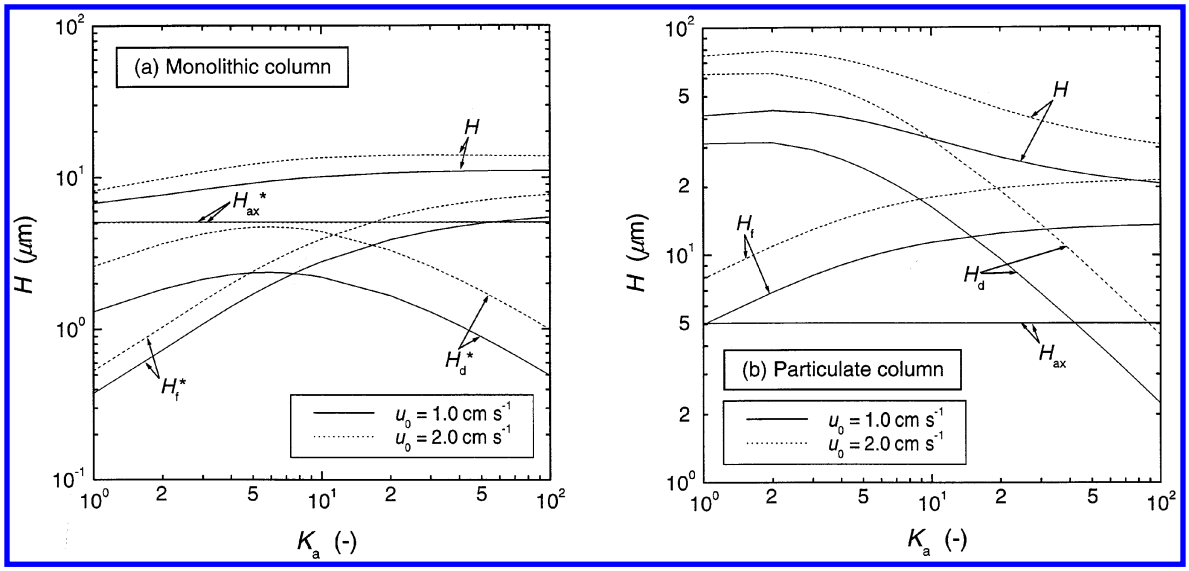

Figure 6. Contributions of each mass transfer process in (a) the hypothetical monolithic column (H^*_{ax}, H^*_f, and H^*_d) and (b) the hypothetical particulate column (H_{ax}, H_f, and H_d) to the correlation between the height equivalent to a theoretical plate and the adsorption equilibrium constant at $u_0 = 1.0$ and 2.0 cm s^{-1}.

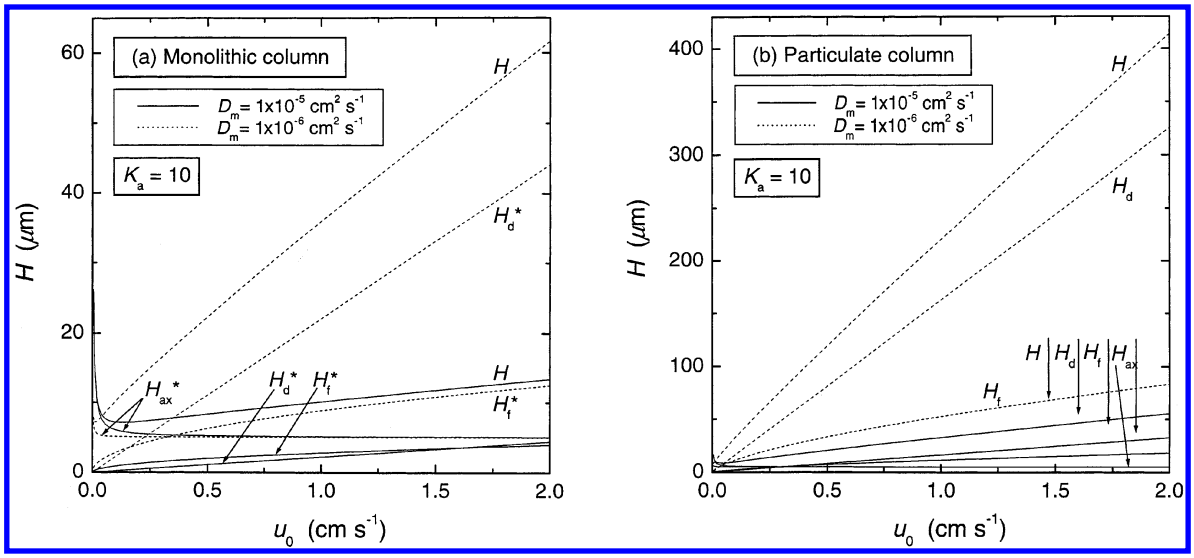

Figure 7. Contributions of each mass transfer process in (a) the hypothetical monolithic column (H^*_{ax}, H^*_f, and H^*_d) and (b) the hypothetical particulate column (H_{ax}, H_f, and H_d) to the correlation between the height equivalent to a theoretical plate and the superficial velocity of the mobile phase at $D_m = 1 \times 10^{-5}$ and 1×10^{-6} cm^2 s^{-1}.

on the relationship between H and u_0 for the monolithic and the conventional packed column, respectively. The correlation between H and u_0 was calculated assuming successively $D_m = 1 \times 10^{-5}$ and 1×10^{-6} cm^2 s^{-1}. As described earlier, the values of D_p and D_s were assumed to be one tenth of D_m.

In Figure 7a, the value of H at $u_0 = 2.0$ cm s^{-1} increases nearly 5-fold when D_m decreases by a factor ten. This phenomenon is primarily due to the increase in H^*_d, which is more sensitive to the change in the diffusivity of the sample compound than H^*_f. By contrast, a decrease in D_m causes an improvement of the column efficiency in the low flow velocity range. However, the contribution of H^*_{ax} is relatively small at $D_m = 1 \times 10^{-6}$ cm^2 s^{-1} and it is almost independent of the value of D_m at high flow rates. Similar changes in the HETP are observed in Figure 7b. The influence of a variation of D_m is more important for the packed column. At $u_0 = 2.0$ cm s^{-1}, the value of H is about 7 times larger at $D_m = 1 \times 10^{-6}$ cm^2 s^{-1} than at $D_m = 1 \times 10^{-5}$ cm^2 s^{-1}. Similar to the results in Figure 7a, the contribution H_d to H is predominant, although the values of H and H_d in Figure 7b are about 1 order of magnitude larger than those in Figure 7a.

The results shown in Figures 3 and 4a suggest that the efficiency of monolithic columns depends only weakly on u_0 and K_a. By contrast with the conventional result obtained with packed columns, their efficiency improves slightly with decreasing K_a. On the other hand, a decrease in the diffusivity of the sample compound provides an important reduction of the column efficiency (Figure 7a), the increase in H arising primarily from the increase in H_d. These results provide useful information concerning the ideal structure of the continuous porous packing material for chromatographic separations of macromolecules. Minimizing the size and thickness of the stationary phase skeleton will contribute to a reduction of the mass transfer resistance in the stationary phase.

Figure 8a,b illustrates the influence of D_m on the relationship between H and K_a. These figures show that H increases with decreasing D_m, irrespective of K_a. The magnitude of the decrease in column efficiency is more important for the packed than for

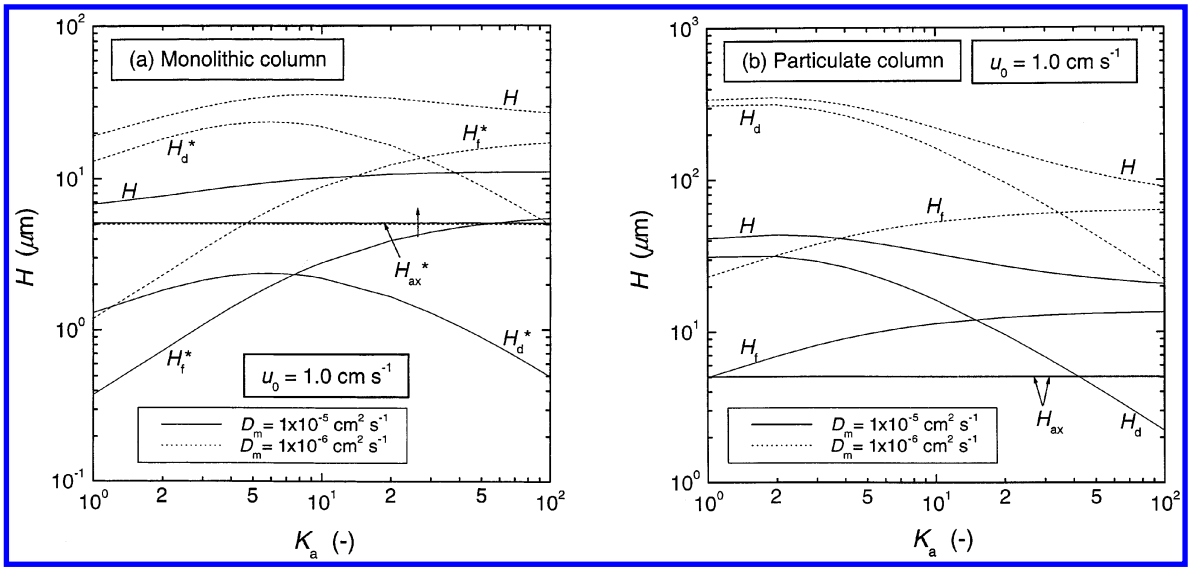

Figure 8. Contributions of each mass transfer process in (a) the hypothetical monolithic column (H^*_{ax}, H^*_f, and H^*_d) and (b) the hypothetical particulate column (H_{ax}, H_f, and H_d) to the correlation between the height equivalent to a theoretical plate and the adsorption equilibrium constant at $D_m = 1 \times 10^{-5}$ and 1×10^{-6} cm^2 s^{-1}.

the monolithic column. The curves describing the contributions H_f and H_d are almost parallel at $D_m = 1 \times 10^{-5}$ and 1×10^{-6} cm^2 s^{-1} in Figure 8a,b. On the other hand, the contribution of H_{ax} is independent of D_m.

Conclusion

Equations relating the peak moments and the parameters characterizing the retention equilibrium and the mass transfer kinetics in monolithic columns were derived by solving the basic equations of the general rate model of chromatography in the Laplace domain. It was assumed that the unit structure of the continuous porous packing material in monolithic columns consists of a cylindrical fiber of stationary phase (including meso- or micropores), surrounded by a through-macropore space filled with mobile phase.

The moment equations derived for monolithic columns were compared with those for conventional columns packed with spherical particles. Hypothetical calculations using these moment equations were made on typical columns of both types. The characteristics of the two types of columns were compared with experimental observations reported in the literature. Calculated and experimental characteristics of the chromatographic behavior of silica monolithic columns were found to be in excellent agreement, suggesting the validity of the new moment equations. Original information was obtained on the correlation between column efficiency on one hand, flow velocity, retention, and diffusivity on the other, particularly regarding the contributions of the three sources of mass transfer resistance in the columns to the HETP and the second central moment of the peaks. Monolithic columns were found to be more efficient than packed columns because their skeleton is thinner and mass transfer across the stationary phase must take place over shorter distances than for columns packed with particles. This property makes them particularly attractive for the separation of macromolecules, especially biomacromolecules.

The new moment equations could be useful for detailed analyses on retention equilibria and mass transfer kinetics in monolithic columns used for chromatographic separations. However, these equations must be validated by systematic comparisons between their predictions and a sufficiently vast body of experimental data. These moment equations are also applicable to kinetic studies of mass transfer phenomena in gas−solid and liquid−solid adsorption, in the cases in which the adsorbent structure has a cylindrical shape, such as activated carbon fibers.

Acknowledgment. This work was supported in part by a Grant-in-Aids for Scientific Research (No. 12640581) from the Ministry of Education, Science and Culture, Japan; by Grant CHE-00-70548 of the National Science Foundation; and by the cooperative agreement between the University of Tennessee and the Oak Ridge National Laboratory.

List of Symbols

$A(p)$: defined in eq 11 (s^{-1})
A_s: ratio of the surface area of the stationary phase skeleton to the column volume (cm^{-1})
A': coefficient of the van Deemter equation (eq 60) (cm)
Bi: Biot number defined in eq 17
$B(p)$: defined in eq 13 (cm^{-2})
$B(z)$: arbitrary function of z
B_0: integration constant in eq 21
B': coefficient of the van Deemter equation (eq 60) (cm^2 s^{-1})
C: concentration of the sample molecules in the through-macropore space (g cm^{-3})
C_i: concentration of the sample molecules within the mesopores inside the stationary phase skeleton (g cm^{-3})
C_0: sample concentration in the injected pulse (g cm^{-3})
C_1: arbitrary constant in eq 12 (g cm^{-3})
C': coefficient of the van Deemter equation (eq 60) (s)
d_p: particle diameter (μm)
d^*_p: diameter of imaginary stationary phase particles corresponding to the size of the through-macropores in the monolithic column (μm)
D_e: diffusion coefficient of the sample molecules in the stationary phase materials (cm^2 s^{-1})
D_L: axial dispersion coefficient (cm^2 s^{-1})
D^*_L: apparent axial dispersion coefficient calculated by eq 50 using d^*_p (cm^2 s^{-1})
D_p: pore diffusivity (cm^2 s^{-1})
D_s: surface diffusion coefficient (cm^2 s^{-1})

$E(p)$: defined in eq 15
$F(p)$: defined in eq 16
$G(p)$: defined in eq 20 (s^{-1})
H: height equivalent to a theoretical plate (mm)
H_{ax}, H_f, H_d: defined in eqs 62 - - 64 (μm)
H^*_{ax}, H^*_f, H^*_d: defined in eqs 57 - - 59 (μm)
k_a: adsorption rate constant (s^{-1})
k_f: external mass transfer coefficient (cm s^{-1})
K_a: adsorption equilibrium constant
m_n: nth moment of chromatographic peak defined in eq 27 (g cm^{-3} s^n)
$M(p)$: defined in eq 22 (cm^{-1})
N_i: mass flux of the sample molecules from the mobile phase stagnant in the mesopore space to the surface of the stationary phase (g cm^{-3} s^{-1})
$N(p)$: defined in eq 36
N_0: mass flux of the sample molecules from the mobile phase to the external surface of the silica skeleton (g cm^{-2} s^{-1})
p: Laplace transform variable (s^{-1})
q: sample concentration adsorbed on the stationary phase (g cm^{-3})
r: radial distance from the center of the stationary phase cylinder (mm)
Re: Reynolds number
R_p: radius of the spherical stationary phase particles (μm)
R_{ss}: radius of the cylindrical stationary phase skeleton (μm)
Sc: Schmidt number
Sh: Sherwood number
t: time (s)
u: interstitial velocity (cm s^{-1})
u_0: superficial velocity (cm s^{-1})
z: longitudinal distance along the column (cm)

Greek symbols

δ_0: defined in eq 56
δ_{ax}, δ, δ_d: defined in eqs 68−70 (s^2)
δ^*_{ax}, δ^*_f, δ^*_d defined in eqs 65−67 (s^2)
ϵ: void fraction (external porosity) of the column
ϵ_p: internal porosity of the stationary phase materials
γ_1, γ_2: geometrical constants in eq 50
η: viscosity (Pa s)
μ_n: nth absolute moment (s^n)
μ_n': nth central moment (s^n)
μ_0: zeroth reduced moment
μ_1: first absolute moment (s)
μ_2': second central moment (s^2)
ρ: density (g cm^{-3})
τ: injection time of sample pulse (s)

References and Notes

(1) Svec, F.; Fréchet, J. M. J. *Anal. Chem.* **1992**, *64*, 820.
(2) Wang, Q. C.; Svec, F.; Fréchet, J. M. *Anal. Chem.* **1993**, *65*, 2243.
(3) Hjertén, S.; Nakazato, K.; Mohammad, J.; Eaker, D. *Chromatographia* **1993**, *37*, 287.
(4) Li, Y.-M.; Liao, J.-L.; Nakazato, K.; Mohammad, J.; Terenius, L.; Hjertén, S. *Anal. Biochem.* **1994**, *223*, 153.
(5) Petro, M.; Svec, F.; Gitsov, I.; Fréchet, J. M. J. *Anal. Chem.* **1996**, *68*, 315.
(6) Peters, E. C.; Petro, M.; Svec, F.; Fréchet, J. M. J. *Anal. Chem.* **1997**, *69*, 3646.
(7) Peters, E. C.; Petro, M.; Svec, F.; Fréchet, J. M. J. *Anal. Chem.* **1998**, *70*, 0, 2288.
(8) Peters, E. C.; Petro, M.; Svec, F.; Fréchet, J. M. J. *Anal. Chem.* **1998**, *70*, 2296.
(9) Minakuchi, H.; Nakanishi, K.; Soga, N.; Ishizuka, N.; Tanaka, N. *Anal. Chem.* **1996**, *68*, 3498.
(10) Minakuchi, H.; Nakanishi, K.; Soga, N.; Ishizuka, N.; Tanaka, N. *J. Chromatogr. A* **1997**, *762*, 135.
(11) Minakuchi, H.; Nakanishi, K.; Soga, N.; Ishizuka, N.; Tanaka, N. *J. Chromatogr. A* **1998**, *797*, 121.
(12) Ishizuka, N.; Minakuchi, H.; Nakanishi, K.; Soga, N.; Tanaka, N. *J. Chromatogr. A* **1998**, *797*, 133.
(13) Minakuchi, H.; Ishizuka, N.; Nakanishi, K.; Soga, N.; Tanaka, N. *J. Chromatogr. A* **1998**, *828*, 83.
(14) Ishizuka, N.; Minakuchi, H.; Nakanishi, K.; Soga, N.; Nagayama, H.; Hosoya, K.; Tanaka, N. *Anal. Chem.* **2000**, *72*, 1275.
(15) Cabrera, K.; Lubda, D.; Eggenweiler, H.-M.; Minakuchi, H.; Nakanishi, K. *J. High Resolut. Chromatogr.* **2000**, *23*, 93.
(16) Nakanishi, K.; Soga, N. *J. Am. Ceram. Soc.* **1991**, *74*, 2518.
(17) Nakanishi, K.; Soga, N. *J. Non-Cryst. Sol.* **1992**, *139*, 1.
(18) Nakanishi, K.; Soga, N. *J. Non-Cryst. Sol.* **1992**, *139*, 14.
(19) Kucera, E. *J. Chromatogr.* **1965**, *19*, 237.
(20) Kubin, M. *Collect. Czech Chem. Commun.* **1965**, *30*, 2900.
(21) Grushka, E.; Myers, M. N.; Schettler, P. D.; Giddings, J. C. *Anal. Chem.* **1969**, *41*, 889.
(22) Grushka, E. *J. Phys. Chem.* **1972**, *76*, 2586.
(23) Guiochon, G.; Golshan-Shirazi, S.; Katti, A. M. *Fundamentals of Preparative and Nonlinear Chromatography*; Academic Press: Boston, 1994.
(24) Suzuki, M. *Adsorption Engineering*; Kodansha/Elsevier: Tokyo/Amsterdam, 1990.
(25) Ruthven, D. M. *Principles of Adsorption & Adsorption Processes*; John Wiley and Sons: New York, 1984.
(26) Suzuki, M.: Smith, J. M. *Chem. Eng. Sci.* **1971**, *26*, 221.
(27) Suzuki, M.: Smith, J. M. *J. Chem. Eng. Jpn.* **1973**, *6*, 540.
(28) Suzuki, M.: Smith, J. M. *Adv. Chromatogr.* **1975**, *13*, 213.
(29) Miyabe, K.; Guiochon, G. *Adv, Chromatography* **2000**, *40*, 1.
(30) Miyabe, K.; Guiochon, G. *Anal. Chem.* **1999**, *71*, 889.
(31) Miyabe, K.; Guiochon, G. *J. Phys. Chem. B* **1999**, *103*, 11086.
(32) Miyabe, K.; Guiochon, G. *Anal. Chem.* **2000**, *72*, 1475.
(33) Miyabe, K.; Guiochon, G. *J. Chromatogr. A* **2000**, *903*, 1.
(34) Miyabe, K.; Guiochon, G. *Anal. Chem.* **2001**, *73*, 3096.
(35) Miyabe, K.; Guiochon, G. *J. Chromatogr. A* **2001**, *919*, 231.
(36) Miyabe, K.; Guiochon, G. *J. Phys. Chem. B* **2001**, *105*, 9202.
(37) Giddings, J. C. *Dynamics of Chromatography, Part I, Principles and Theory*; Marcel Dekker: New York, 1965.
(38) Knox, J. H.; Scott, H. P. *J. Chromatogr.* **1984**, *316*, 311.
(39) Frevel, L. K.; Kressley, L. J. *Anal. Chem.* **1963**, *35*, 1492.
(40) Bird, R. B.; Stewart, W. E.; Lightfoot, E. N. *Transport Phenomena*; John Wiley & Sons: New York, 2002.
(41) Kataoka, T.; Yoshida, H.; Ueyama, K. *J. Chem. Eng. Jpn.* **1972**, *5*, 132.
(42) Wilson, E. J.; Geankoplis, C. J. *Ind. Eng. Chem. Fundam.* **1966**, *5*, 9.
(43) Miyabe, K.; Guiochon, G. *Anal. Chem.* **2000**, *72*, 5162.
(44) Knox, J. H. *J. Chromatogr. A* **1999**, *831*, 3.
(45) Guiochon, G.; Farkas, T.; Guan-Sajonz, H.; Koh, J.-H.; Sarker, M.; Stanley, B. J.; Yun, T. *J. Chromatogr. A* **1997**, *762*, 83.
(46) Horne, D. S.; Knox, J. H.; McLaren, L. *Sep. Sci.* **1966**, *1*, 531.
(47) Knox, J. H.; Laird, G. L.; Raven, P. A. *J. Chromatogr.* **1976**, *122*, 129.
(48) Eon, C. H. *J. Chromatogr.* **1978**, *149*, 29.
(49) Baur, J. E.; Kristensen, E. W.; Wightman, R. M. *Anal. Chem.* **1988**, *60*, 2334.
(50) Baur, J. E.; Wightman, R. M. *J. Chromatogr.* **1989**, *482*, 65.
(51) Farkas, T.; Chambers, J. Q.; Guiochon, G. *J. Chromatogr. A* **1994**, *679*, 231.
(52) Farkas, T.; Sepaniak, M. J.; Guiochon, G. *J. Chromatogr. A* **1996**, *740*, 169.
(53) Farkas, T.; Guiochon, G. *Anal. Chem.* **1997**, *69*, 4592.
(54) Farkas, T.; Sepaniak, M. J.; Guiochon, G. *AIChE J.* **1997**, *43*, 1964.
(55) Baumeister, E.; Klose, U.; Albert, K.; Bayer, E.; Guiochon, G. *J. Chromatogr. A* **1995**, *694*, 321.
(56) Tallarek, U.; Albert, K.; Bayer, E.; Guiochon, G. *AIChE J.* **1996**, *42*, 3041.
(57) Tallarek, U.; Bayer, E.; van Dusschoten, D.; Scheenen, T.; Van As, H.; Guiochon, G.; Neue, U. D. *AIChE J.* **1998**, *44*, 1962.
(58) Tallarek, U.; Bayer, E.; Guiochon, G. *J. Am. Chem. Soc.* **1998**, *120*, 1494.
(59) Yun, T.; Guiochon, G. *J. Chromatogr. A* **1994**, *672*, 1.
(60) Yun, T.; Guiochon, G. *J. Chromatogr. A* **1996**, *734*, 97.
(61) Yun, T.; Guiochon, G. *J. Chromatogr. A* **1997**, *760*, 17.